Dynamics of biological molecules irradiated by short x-ray pulses

Stefan P. Hau-Riege, Richard A. London, and Abraham Szoke
Lawrence Livermore National Laboratory, Livermore, California 94551, USA
(Received 16 October 2003; published 18 May 2004)

Very short and intense x-ray pulses can be used for diffraction imaging of single biological molecules. Inevitably, x-ray absorption initiates damage that degrades the molecule's image. This paper presents a continuum model of the physics that leads to damage when a small particle absorbs a large x-ray dose. The main processes are found to be ionization and Coulomb-force driven atomic motion. Trapping of electrons, Debye shielding, and nonuniform collisional ionization all have a significant effect on the overall damage kinetics.

DOI: 10.1103/PhysRevE.69.051906 PACS number(s): 82.53.Ps, 52.30.−q, 52.65.−y

I. INTRODUCTION

The principal tool for structure determination of biological molecules is x-ray crystallography. Since many biologically important molecules have been very difficult or as-yet impossible to crystallize, it is highly desirable to develop methods to determine structures of *noncrystalline* single molecules [1]. Whereas radiation damage is mitigated in crystals by utilizing coherent scattering from a large number of identical molecules, damage severely limits image resolution of noncrystalline samples [2,3]. It has been suggested that extremely short x-ray pulses can be used to image single molecules before the damage takes place. This idea of flash imaging was first suggested by Solem *et al.* [4,5], and extended to atomic resolution imaging of single biological molecules by Neutze *et al.* [1].

Future x-ray free-electron lasers (XFELs) [6,7] hold the promise to provide the necessary short pulses to overcome the damage limitations and enable the determination of molecular structure from single molecules [1]. XFELs are expected to provide pulses of soft and hard x-ray photons with pulse durations in the range of 10–300 fs and brightness more than ten orders of magnitude larger than current x-ray sources [3,8,9]. In the simplest scenario, individual identical molecules will be exposed to XFEL pulses one-by-one in random, unknown orientation. Since the measured diffraction patterns will be very noisy, due to photon counting statistics, the limiting step will be the ability to classify the diffraction patterns according to their orientation. After classification, the diffraction patterns can be averaged to improve the signal-to-noise ratio [10], and the class averages of diffraction patterns can be assembled into a single three-dimensional diffraction pattern. Finally, the real space molecular image can be calculated using image reconstruction techniques [11,12].

Although the extreme brightness of XFEL pulses helps to ameliorate the noise problem in classification, the x-ray intensity is still limited by the damage to the sample in a single XFEL radiation pulse. Only with sufficiently short and intense pulses can diffraction images be recorded before the structure has undergone significant radiation-induced changes. In this paper we will address the key question of how short and how intense the XFEL pulses must be to accomplish this goal.

Calculations on the dynamics of biological molecules irradiated by high-intensity short-pulse x-rays have recently been presented by Neutze *et al.* [1] and Jurek *et al.* [13]. They used detailed molecular dynamics codes to calculate the atomic motions and the resulting degradation in image resolution for a few biological molecules. In the present work, we consider a simpler dynamics model, but add the effect of trapped electrons, which Neutze *et al.* left out. Jurek *et al.* did consider this effect, but they were limited to a size range of 50–1500 atoms per molecule, corresponding to a radius of 15 Å or less. Our approach allows the calculation of much larger molecules, at the expense of neglecting some details of atomic motion. Specifically, we neglect the changes in atomic forces caused by the changed electron distribution when atoms get ionized.

In this paper, we introduce a simple, one-dimensional spherical model for the dynamics of short pulse x-ray irradiated molecules that includes approximate descriptions of the dominant physical processes and which can be easily used to survey a wide range of molecular sizes, compositions, and image resolutions. We present an overview of the physical processes for the dynamics of an x-ray irradiated biological molecule in Sec II, describe our models for these processes in Sec. III, and then present and analyze a characteristic computer simulation based on this model in Sec. IV. We finally report and discuss the results of calculations for a wide range of molecular sizes and x-ray intensities in Secs. V and VI. The Appendix contains an analytic solution for a simplified dynamics model that is useful for checking numerical simulations and for obtaining insight into the more detailed calculations.

II. OVERVIEW OF PHYSICAL PROCESSES

We consider the sequence of events when an intense x-ray pulse of wavelength of ~1 Å irradiates a biological molecule. Only a small fraction of the x-rays interact with the molecule. The "useful" photons are those that scatter elastically and produce the diffraction pattern. However, the dominant interaction is *K*-shell photoionization of the atoms in the molecule, which leads to damage. It produces electrons with energy close to the incident photon energy (~12 keV). Within several femtoseconds, the *K*-shell holes of the nonhydrogenic atoms (C, N, O, etc.) decay, mainly by emitting Auger electrons with relatively low energies (250–500 eV) [14].

Early in the x-ray pulse, most of the electrons escape the molecule. The escaping electrons leave behind a net positive charge. This charge quickly becomes large enough so that the Auger electrons become electrostatically trapped in the molecule. Even the photoelectrons become trapped for larger molecules. It is instructive to consider a few numerical examples of the trapping energy. Electrons emitted perpendicular to the surface of a homogeneous, spherically symmetric charged molecule of radius R are trapped if their kinetic energy is smaller than $e^2R^2n/3\varepsilon_0$, where ε_0 is the permittivity of vacuum, e is the elementary charge, and n is the charge number density. Somewhat higher-energy electrons are trapped from the interior of the molecule. For typical x-ray fluences necessary for imaging (see Sec. V), approximately half of all of the atoms become photoionized. Assuming all photoelectrons escape, this results in $n \approx 0.06/\text{Å}^3$. For this charge number density and a typical protein composition (see Sec. V), electrons of energy 250 eV or less are trapped by molecules of radius 8 Å or larger. Since most molecules of interest are larger than 8 Å, we conclude that most Auger electrons will be trapped. Assuming the same charge density, 12 keV photoelectrons will be trapped when $R \geqslant 58$ Å.

Both escaping and trapped photoelectrons produce secondary electrons through collisional ionization of atoms. The escaping photoelectrons produce at most a few secondaries, while trapped Auger and photoelectrons produce the majority of the secondaries. For the abundant elements, C, N, and O, the cross section is largest for ionization of the outer L-shell electrons. Since the ionization energy of L-shell electrons is rather low [15], each trapped secondary electron can induce multiple ionization events. This has been described in detail for large, cold carbon samples by Ziaja *et al.* [16]. The energy of the secondaries is typically less than 100 eV, so that, according to the estimate above, most of the secondary electrons will be trapped in the molecule. Most atomic recombination processes such as radiative recombination which dominate at low electron densities occur on time scales that are longer than the x-ray pulse length. However, for certain beam parameters the electron and ion densities become large enough so that three-body recombination effects in which an ion captures an electron with the binding energy being absorbed by a second electron are important.

The trapped electrons collide with each other very frequently ($\sim 1/\text{fs}$) and, after a few collisions, their energy distribution becomes Maxwellian. After a somewhat longer time, they relax in position to form a neutralizing cloud around the positively charged ions. Such a collection of electrons and ions resemble an electron-ion plasma, and the neutralization of the charge is similar to Debye shielding. The particle then assumes a roughly two-zone structure, consisting of a neutral core and a positively charged outer shell, which extends to the boundary of the particle. On a longer time scale of order 10 fs, the repulsive electrostatic forces between the ions cause a macroscopic motion of the whole molecule, called a Coulomb explosion. This motion has been previously illustrated using molecular dynamic simulation methods in Ref. [1].

III. DESCRIPTION OF THE MODEL

A. Continuum approximation

The basic assumption of the model is that the molecule can be described by a continuum of matter rather than considering the individual atoms, as in the molecular dynamics approach. This is expected to provide an adequate description of the average effects of x-ray material interaction and atomic motion when the samples contain many atoms. We further assume that the particle is spherically symmetric, reducing the mathematical model to one dimension plus time. We assume that the motion of the atoms within the molecule is solely in the radial direction.

The electrons and the atoms are treated as separate, structureless, fluids that interact through the Coulomb force and ionization processes. The short-range electron-electron interaction is treated as a hydrodynamic pressure, and the long-range electron-electron and electron-ion Coulomb interaction is determined from the continuous net charge of the electrons and ions. In this model, all forces act radially. We further assume that the trapped electrons are thermalized among themselves, and that they are inertia free, so that they quickly relax to a force-free spatial equilibrium. Finally, the x-ray matter interaction, atomic ionization processes, and energy of the trapped electrons are described by time-dependent rate equations.

In the following Secs. III B and III E , we expand on these issues further, give a more detailed description of the model, and provide justifications for our assumptions.

B. Treatment of trapped electrons

The electrons are divided into escaped, trapped, and bound electrons. According to the estimates of the trapping energy presented in Sec. II, we assume that all secondary and Auger electrons are trapped, whereas for each photoelectron we determine whether it is trapped or not depending on its kinetic energy relative to the local escape energy.

For certain beam parameters the electron and ion densities become large enough so that three-body recombination effects are important. We included this effect in a subset of the simulations. We only include recombination into the L shell, since higher shells are likely to be merged into the continuum due to the higher electron density.

On a time scale of a few femtoseconds, the trapped electrons collide with each other and produce a Maxwellian energy distribution. In our model we assume that this thermalization occurs instantaneously. As long as there are no transient processes shorter than 3–4 fs this is a good approximation. The trapped electrons are treated as an ideal fluid, with a temperature proportional to their average kinetic energy: $T_e = 2\langle E_t \rangle / 3k$, where k is the Boltzmann constant. The atoms stay cold since the electron-atom collisional energy transfer time is much longer than the pulse length.

We further assume that the electrons quickly relax to a force-free spatial equilibrium that includes both pressure and electrostatic forces. In reality, the relaxation rate is characterized by the minimum of the plasma frequency and the electron-electron collisional rate. Both are of the order of

1 fs^{-1}, and thus the relaxation may be considered fast. In this approximation, the forces on an electron are the electrostatic force due to the ions F_i, the electrostatic force due to the electrons F_e, and the force due to the pressure gradient, F_p:

$$F_i(r) = -\frac{e^2}{\varepsilon_0 r^2}\int_0^r n_{\mathrm{i}}(r')r'^2 dr', \tag{1}$$

$$F_e(r) = \frac{e^2}{\varepsilon_0 r^2}\int_0^r n_{\mathrm{e}}(r')r'^2 dr', \text{and} \tag{2}$$

$$F_{\mathrm{p}}(r) = -kT_{\mathrm{e}}\frac{1}{n_{\mathrm{e}}(r)}\frac{dn_{\mathrm{e}}(r)}{dr}. \tag{3}$$

Here r is the distance of the electron from the center of the molecule, n_{i} is the ion charge number density, n_{e} is the electron number density, and T_{e} is the electron temperature. The condition for force-free equilibrium is

$$F_{\mathrm{i}} + F_{\mathrm{e}} + F_{\mathrm{p}} = 0. \tag{4}$$

This condition leads to neutralizing the core of the molecule, equivalent to Debye shielding on the molecular scale. As described in more detail in Sec. IV, it is numerically more stable to solve Eq. (4) in terms of the space-integrated electron and ion density.

C. Atomic motion

The molecule explodes due to a net positive charge left by escaping electrons and the electron pressure. The ions move in response to the electrostatic force from both the electrons and the other ions. We ignore the initial molecular binding forces since they are very small compared to the forces generated by even moderate x-ray ionization. The radial acceleration is given by

$$a(r) = \frac{1}{\varepsilon_0 \rho(r) r^2}[n_{\mathrm{i}}(r) - n_{\mathrm{e}}(r)]\int_0^{\mathrm{r}} r'^2[n_{\mathrm{i}}(r') - n_{\mathrm{e}}(r')]dr', \tag{5}$$

where ρ is the mass density.

D. Description of ionization processes through rate equations

Consistent with our continuum model approach, we calculate the number and total energy of trapped electrons, and the ionization states of the atoms in the molecule using time-dependent rate equations. The equations account for three processes: (i) photoionization, (ii) Auger relaxation, and (iii) collisional ionization. The ionization states of each type of atom in the molecule, such as H, C, N, O, etc., are described as space and time-dependent population densities. The ionization rate equations for each element are

$$\frac{dN_{\mathrm{ij}}}{dt} = \sum_{\mathrm{kl}\neq\mathrm{ij}} (R_{\mathrm{kl}\to\mathrm{ij}}N_{\mathrm{kl}} - R_{\mathrm{ij}\to\mathrm{kl}}N_{\mathrm{ij}}), \tag{6}$$

where N_{ij} is the density of atoms with i electrons in the K shell and j electrons in the L shell. We denote this state as (i,j). The total rate of ionization events from state (k,l) to state (i,j) is $R_{\mathrm{kl}\to\mathrm{ij}}$. The values for i, j are limited to $0 \leqslant i \leqslant 2$ and $0 \leqslant j \leqslant (0,4,5,\text{or } 6)$ for (H, C, N, and O). Since we consider only single ionization processes of the K shell (i.e., $i=k$-1 and $j=1$), the rate matrix $R_{\mathrm{kl}\to\mathrm{ij}}$ is actually very sparse. The photoionization rates are

$$R^{\mathrm{ph}}_{\mathrm{kl}\to\mathrm{ij}} = F_{\mathrm{ph}}\sigma^{\mathrm{ph}}_{\mathrm{kl}}, \tag{7}$$

with $i=k$-1 and $j=l$. F_{ph} is the photon flux and $\sigma^{\mathrm{ph}}_{\mathrm{kl}}$ is the photoionization cross section [17]. The Auger decay rates are

$$R^{\mathrm{Auger}}_{\mathrm{kl}\to\mathrm{ij}} = \frac{1}{\tau_{\mathrm{kl}}}, \tag{8}$$

with $i=k+1$ and $j=1-2$, and τ_{kl} is the Auger lifetime of state (k,l) [14]. The rates for secondary ionization of the trapped electrons are

$$R^{\mathrm{coll}}_{\mathrm{kl}\to\mathrm{ij}} = N_{\mathrm{tr}}\langle\sigma^{\mathrm{coll}}_{\mathrm{kl}\to\mathrm{ij}}v_{\mathrm{e}}\rangle, \tag{9}$$

with $i=k-1$ and $j=0$ if $l=0$, and $i=k$ and $j=l-1$ if $l>0$. N_{tr} is the number density of trapped electrons, and $\langle\sigma^{\mathrm{coll}}_{\mathrm{kl}\to\mathrm{ij}}v_{\mathrm{e}}\rangle$ is the average of the collisional ionization cross sections multiplied by the electron velocity [18,19]. In our approximation, the average is taken over the Maxwellian electron distribution function. We assume that all Auger and other secondary electrons are trapped. Finally, the rates for the secondary ionization by escaping photoelectrons is given by

$$R^{\mathrm{pe}}_{\mathrm{kl}\to\mathrm{ij}}(r) = \langle r\rangle\sigma^{\mathrm{coll}}_{\mathrm{kl}\to\mathrm{ij}}\sum_{\mathrm{mn}} N_{\mathrm{mn}}R^{\mathrm{phl}}_{\mathrm{mn}\to\mathrm{op}}p_{\mathrm{esc}}(r), \tag{10}$$

with $i=k-1$ and $j=0$ if $l=0$, and $i=k$ and $j=l-1$ if $l>0$; and with $o=m-1$ and $p=n$. The sum is the rate of the generation of photoelectrons per unit volume that escape the molecule. $\sigma^{\mathrm{coll}}_{\mathrm{kl}\to\mathrm{ij}}$ is the ionization cross section at the photoelectron energy E^{photon} and $\langle\mathrm{r}\rangle$ is the average distance a photoelectron travels through the molecule before escaping, taken to be the molecule radius at the beginning of the explosion. The escape probability p_{esc}, is used to isolate the ionization by escaping photoelectrons from that due to trapped photoelectrons. The contribution from the latter is treated with the trapped electrons described by Eq. (9) above. If the photoelectrons escape from the shell at radius r, $p_{\mathrm{esc}}(r)=1$, otherwise $p_{\mathrm{esc}}(r)=0$.

The total rate of ionization events is then

$$R_{\mathrm{kl}\to\mathrm{ij}} = R^{\mathrm{ph}}_{\mathrm{kl}\to\mathrm{ij}} + R^{\mathrm{Auger}}_{\mathrm{kl}\to\mathrm{ij}} + R^{\mathrm{coll}}_{\mathrm{kl}\to\mathrm{ij}} + R^{\mathrm{pe}}_{\mathrm{kl}\to\mathrm{ij}}. \tag{11}$$

The rate equation for the number density of trapped electrons is

$$\frac{dN_{\mathrm{tr}}}{dt} = \sum_{\mathrm{ij}\neq\mathrm{kl}} \{[R^{\mathrm{Auger}}_{\mathrm{kl}\to\mathrm{ij}} + R^{\mathrm{coll}}_{\mathrm{kl}\to\mathrm{ij}} + R^{\mathrm{ph}}_{\mathrm{kl}\to\mathrm{ij}}(1-p_{\mathrm{esc}}) + R^{\mathrm{pe}}_{\mathrm{kl}\to\mathrm{ij}}]N_{\mathrm{ij}}\}, \tag{12}$$

where r is the molecule radius. Finally, the rate equation for the energy density of the trapped electrons E_{tr} is

$$\frac{dE_{\rm tr}}{dt} = \sum_{ij\neq kl} R^{\rm Auger}_{kl\to ij} N_{ij} E^{\rm Auger}_{ij} - \sum_{ij\neq kl} R^{\rm coll}_{kl\to ij} N_{ij} E^{\rm coll}_{ij} + R^{\rm ph}_{kl\to ij}(1-p_{\rm esc}) N_{ij} E^{\rm photon} + R^{\rm pe}_{kl\to ij} N_{ij} E^{\rm pe}_{ij}, \quad (13)$$

where $E^{\rm Auger}_{ij}$ is the energy of the $(i,j)\to(k,l)$ Auger transition [14], $E^{\rm coll}_{ij}$ is the binding energy that needs to be expended for the $(i,j)\to(k,l)$ transition during secondary collisional ionization, and $E^{\rm pe}_{ij}$ is the energy of the secondary electrons induced by the escaping photoelectron, and is assumed to be approximately three times the average ionization energy, or about 25 eV [20].

E. Omissions

For completeness, we summarize the most important omissions in our model. Consistent with the continuum approximation, we do not describe the details of interatomic forces, such as the van der Waals force and other binding forces that determine the initial molecular structure. Therefore, we do not accurately model any atomic motion that results from the disruption of these forces when the molecule begins to get ionized. We also do not consider that different atomic species (e.g., H and C) from the same vicinity of the molecule may move at different speeds. In reality, hydrogen atoms may move much faster, particularly from the surface of the molecule, as described for diatomic molecules by Chelkowski and Bandrauk (1995) [21]. However, those atoms in the interior of the molecule will be prevented from moving faster than the bulk by collisions. In any case, the movement of hydrogen atoms is not very important for the application of x-ray diffraction since they are weak x-ray scatterers and the molecular structure can be determined from the positions of the heavier atoms (C, N, O, etc.).

Associated with the ideal electron gas approximation, we neglect the time-dependent relaxation processes and the possibility of a non-Maxwellian electron distribution. One such effect is that barely trapped electrons (particularly photoelectrons) will spend some time orbiting outside the molecule before they thermalize. This may slightly reduce the collisional ionization rate. By using cross sections derived for isolated atoms, we ignore the molecular effects on the collisional ionization rates and any dynamical change in such effects as the molecule begins to explode. These effects may be important for low electron energies ($<$100 eV) where the de Broglie wavelength approaches the interatomic separation and where the electron energy becomes comparable to the valence ionization energy. By comparison of the atomic ionization cross sections for carbon to cross sections calculated for diamond by Ziaja *et al.* (2004) [22], we estimate that errors less than a factor of 2 might be expected in the low-energy regime. We assume radial trajectories in calculating electron trapping. We further neglect any shake-up and shake-off excitations.

Finally, the atomic motions are assumed to be always radial, so the effects of molecular shape and local inhomogeneity are neglected. Although the omissions of our model may affect the motion of atoms on very short lengths ($<$1 Å) and short time scales ($<$2 fs), our model is sufficient to understand the overall dynamics of the damage processes and to give meaningful predictions for the x-ray pulse durations necessary to beat the damage processes.

IV. DESCRIPTION OF COMPUTER SIMULATIONS

We have developed a computer program to solve the equations presented in Sec. III, and thereby to handle arbitrary x-ray pulses, nonhomogeneous radial structures, and to include the effects of trapped electrons. The molecule is divided into equidistant radial zones, i.e., spherical shells. We track the zone boundaries as the molecule expands. We calculate the time-dependent ion motion with a Lagrangean finite differencing scheme [23], using the acceleration given by Eq. (5). We use a solver that is explicit in time and first-order accurate in both time and space.

We use artificial viscosity to prevent zone collapse and to resolve shock waves [23–25]. The artificial viscosity q was taken to be

$$q = c_1 c_s \rho |\Delta v| + c_2 \rho (\Delta v)^2, \quad (14)$$

where Δv is the velocity difference across a zone, $c_s = (kT_e/M)^{1/2}$ is the sound speed, where M is average atomic mass, and c_1 and c_2 are constants of order unity. They have to be large enough to prevent numerical problems but small enough to not distort the solution. We have chosen $c_1=1$ and $c_2=10$ [25]. Equation (14) is applied only when a zone is being compressed. Otherwise the artificial viscosity is set equal to zero. The radial gradient of the artificial viscosity is taken as an additive term to the nodal acceleration given by Eq. (5).

We solve the rate equations for each zone with explicit, first, order finite differencing. We are primarily concerned with biological molecules that are made up of H, C, N, O, P, and S. For the elements H, C, N, and O, we account for all electrons. For simplicity we treat phosphorous and sulfur as if they had only eight electrons. The remaining electrons of the sulfur and phosphorous atoms are assumed to be stationary.

We used 100 equally spaced radial zones for all simulations, after finding that increasing the number of zones did not change the results by more than 5%. We use a variable time step, Δt, taken as $\Delta t = \Delta x/c_s$, where Δx is the zone width. This is the usual Courant-Friedrichs-Lewy stability condition that, together with the use of artificial viscosity, prevents zone collapse and numerical instability [26]. We further enforce that Δt stays below 4×10^{-4} fs for solving the rate equations without significant numerical error.

During each time step we calculate the equilibrium electron distribution by solving a modified version of Eq. (4). We found that using simple shooting methods to solve the finite-difference equations based on Eq. (4) was numerically unstable. Instead, we wrote Eq. (4) in terms of the integrated densities,

$$\frac{e}{4\pi\varepsilon_0 r^2}(N_i + N_e) + kT_e\left(\frac{N_e''}{N_e'} - \frac{2}{r}\right) = 0, \quad (15)$$

where

$$N_e(r) = -4\pi e \int_0^r n_e(r')r'^2 dr', \tag{16}$$

and

$$N_i(r) = 4\pi e \int_0^r n_i(r')r'^2 dr'. \tag{17}$$

The problem is now a two point boundary value problem with boundary conditions $N_e(0)=0$ and $N_e(\infty)=Q/e$, where Q is the total electron charge. We found that a relaxation method as described in Ref. [27] provides an accurate, numerically stable solution. We then calculate n_e from Eq. (16) by numerical differentiation.

V. RESULTS

A. Standard model

We first illustrate the results of the computer model for an example with typical parameters that will be used in all our simulations except stated otherwise. The chemical stoichiometry is that of the anthrax lethal factor, a particular protein of current interest: $H_{51.61}C_{30.77}N_{8.16}O_{9.40}S_{0.60}$ [28]. Other protein molecules have quite similar composition. We assumed a mass density of $1.35 g/cm^3$ and an initial radius of 60 Å, determined from the maximum distance of atoms from the molecule's center of mass. We use a flat top pulse (i.e., constant flux) of 12 keV photons at a flux of 1.5×10^{11} ph/fs/(100 nm)^2 $=2.88\times10^{21}$ W/cm^2, lasting 20 fs. This corresponds to a fluence of 3×10^{12} ph/(100 nm)^2. This number of photons and focal spot is typical of what is expected of future XFELs, and is the order of magnitude needed to be able to classify diffraction patterns with a resolution of a fraction of a nanometer [10].

B. Ionization

We first compare two simulations with and without trapping and secondary ionization. In the first simulation, we assume that electrons are not trapped, and that the only ionization processes are photoionization, collisional ionization by the escaping electrons, and Auger decay. Figure 1(a) shows the ionization of carbon, the dominant x-ray interacting constituent of biomolecules. Figure 1(b) shows the number of escaped electrons as a function of time. The number of atoms in state (1,4) increases with time due to photoionization of neutral atoms [state (2,4)]. Only a small number of other states are generated by collisional ionization by escaping photoelectrons. By 18 fs about 2/3 of the C atoms have been ionized. Eventually, photoionization will deplete all K-shell electrons. On a time scale of approximately 10 fs, the carbon Auger decay gives rise to an increased number of atoms in state (2,2) at the expense of atoms in state (1,4).

In the second simulation, we used the full model, including electron trapping and secondary ionization. Figures 2(a) through 2(e) show the ionization of H, C, N, O, and S. Even though photoionization is still the initial process, collisional ionization of the valence electrons quickly dominates the behavior. The electrons that strip the valence electrons are predominantly secondary electrons generated through collisional ionization by the escaping photoelectrons and by the Auger electrons. In spite of its low concentration, the contribution from sulfur is quite large because its photoionization and Auger rates are very large. Figure 2 shows that stripping of the heavier elements such as O, N, and S progresses faster that the stripping of C due to higher ionization rates. Figure 3(a) shows the time evolution of the average electron energy. The initial temperature is determined by the energy of the secondaries produced by the escaping photoelectrons. Within the first few femtoseconds, the electron energy quickly drops due to the increasing number of low-energy secondary electrons. This process saturates, and subsequently Auger relaxation of the lighter and more abundant species such as carbon leads to an increase of the average energy. This process also saturates eventually. At approximately 15 fs, the photoelectrons become trapped leading to a large increase in the electron energy. The increase is artificially abrupt due to neglect of nonradial trajectories when calculating the trapping energy. Figure 3(b) shows the number of trapped and escaped electrons as a function of time. Also shown on this graph are the origins of the trapped electrons classified as collisional ionization by trapped electrons, collisional ionization by escaping photoelectrons, Auger relaxation, and photoionization. At 10 fs, 19% of all unbound electrons have been generated by photoionization, 8% by Auger ionization,

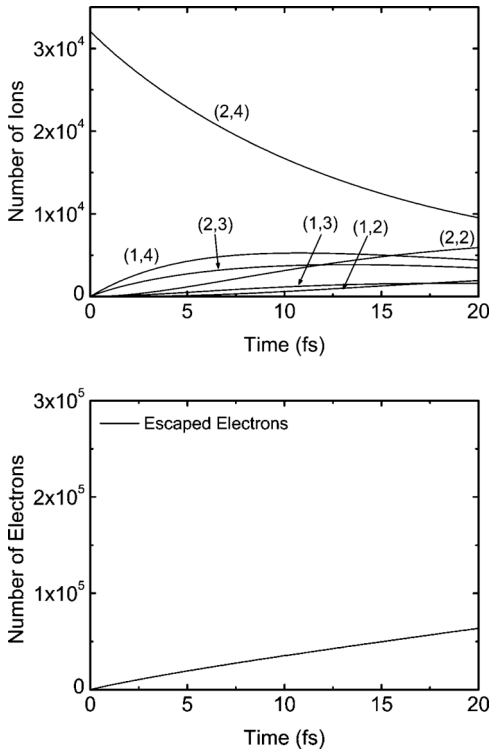

FIG. 1. (a) Ionization of carbon for the case of the full ionization model, but without trapping of electrons. The molecule is of radius 60 Å and is illuminated by a photon pulse of flux 1.5×10^{11} ph/fs/(100 nm)^2 for 20 fs. (i,j) denotes a state with I electrons in the K shell and j electrons in the L shell. Only the states that reach densities of at least 5% of the initial density of the neutral state (2,4) are shown. (b) Number of escaped electrons as a function of time.

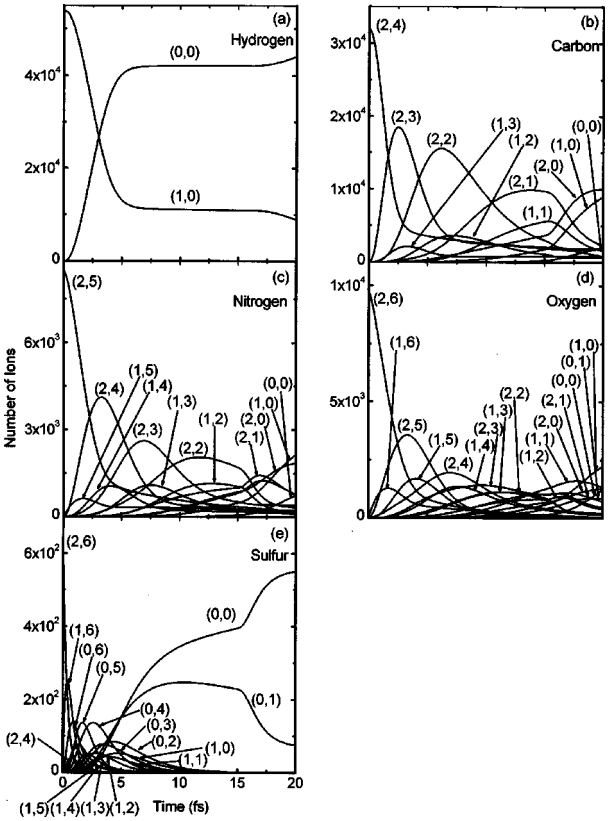

FIG. 2. Ionization of (a) hydrogen, (b) carbon, (c) nitrogen, (d) oxygen, and (e) sulfur using the full ionization model. The molecule is of radius 60 Å and is illuminated by a photon pulse of flux 1.5×10^{11} ph/fs(100 nm)^2 for 20 fs.

and 73% by collisional ionization. At 20 fs, 23% of all unbound electrons have been generated by photoionization, 10% by Auger ionization, and 67% by collisional ionization. In summary, the majority of trapped electrons are generated by cascade processes, i.e., they are secondaries created by other secondary electrons.

We found a pronounced dependence of the ionization time scales on the chemical composition of the particle. Figure 4(a) shows the ionization of carbon for a molecule without sulfur ($H_{51.91}C_{30.87}N_{8.26}O_{9.50}$), and Fig. 4(b) shows the ionization of carbon for a molecule that consists of carbon only. This should be contrasted to the ionization of carbon in a molecule with the standard chemical composition as shown in Fig. 2(b). All three simulations were performed for the same beam parameters, molecule radius, and mass density. These results demonstrate that the heavier elements, such as sulfur, oxygen, or nitrogen, strongly enhance the ionization of biological molecules.

We also performed simulations using parameters similar to the second simulation shown in Figs. 2, 3(a), and 3(b), but including three-body recombination. The recombination rates are calculated from the collisional ionization rates using the principle of detailed balance [29]. We find that three-body recombination has a noticeable but not overwhelming effect on the ionization process: the number of trapped electrons is 32 % lower at 5 fs if three-body recombination is included. In the following calculations, we do not consider recombination processes.

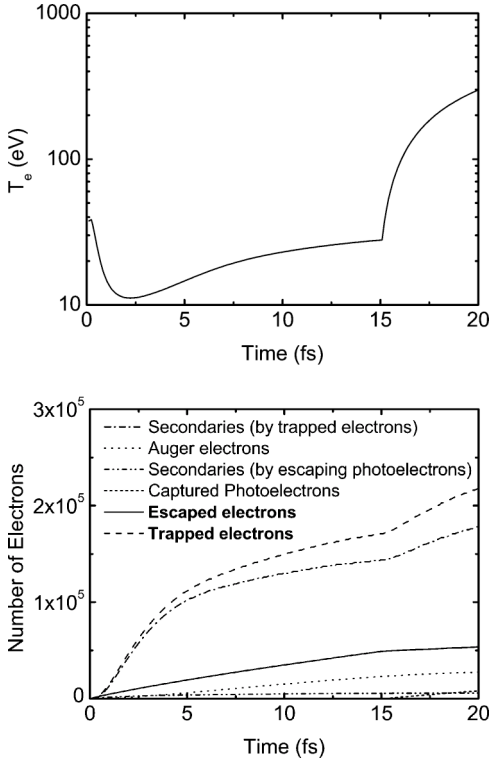

FIG. 3. Time evolution of (a) the average electrons temperature T_e and (b) electron count for the simulations shown in Fig. 2.

C. Electron distribution

Figure 5 shows the radial dependence of the electron density at several times, assuming the force-free equilibrium

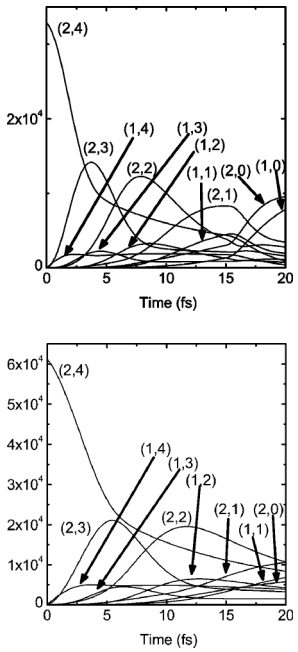

FIG. 4. Ionization of carbon for the case of a 60 Å radius molecule illuminated by a photon pulse of flux 1.5×10^{11} ph/fs(100 nm)^2 for 20 fs. The molecule stoichiometry was (a) $H_{51.91}C_{30.87}N_{8.26}O_{9.50}$ and (b) carbon only.

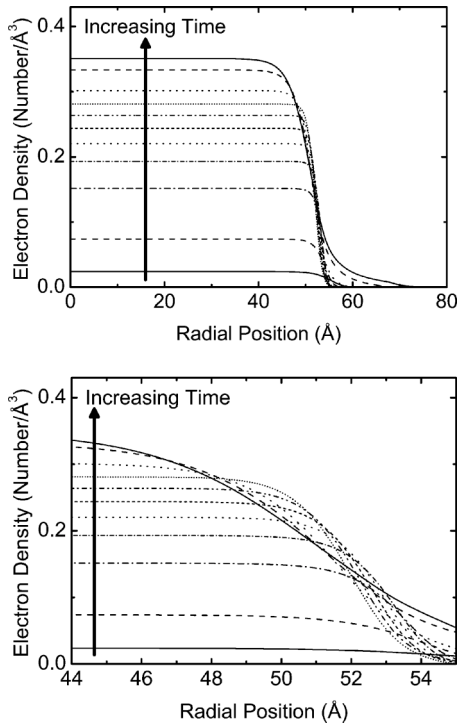

FIG. 5. (a) Radial dependence of the electron density for different times, 1 fs, 2 fs, 4, fs, 6 fs, up to 20 fs. We assumed a 60 Å radius molecule illuminated by a photon pulse of flux 1.5×10^{11}ph/fs/(100 nm)^2 for 20 fs. (b) Close-up of the data shown in (a).

given by Eq. (5). Due to progressing ionization, the electron density near the center of the molecule increases with time. Near the center, the electron charge density closely follows the ion charge density, leading to a neutral molecule core. The electron density drops with increasing radius with a slope depending on the temperature of the electrons and the magnitude of the electrostatic potential. Related to the evolution of the electron temperature shown in Fig. 3(a), the electron distribution first becomes steeper for decreasing temperatures and increasing charge, and then becomes shallower again once the photoelectrons are trapped and the temperature rises.

D. Coulomb explosion

In order to verify our computer program we compared it to the analytical solution from the Appendix for the case of a 60 Å-radius molecule containing only carbon. We assumed that no electrons are trapped, and that the total charge density of 0.22 electrons/Å^3 is initially homogeneous throughout the molecule. Figure 6 shows a comparison of the motion of the radial zones of the molecule calculated numerically and analytically. The results agree to better than 0.1% for all times and positions, giving good confidence in the numerical methods used to solve the equation of motion.

Figure 7 illustrates the outward motion of selected spatial zones of the molecule for the standard case, but with a longer pulse (60 fs versus 20 fs). We see the differentiation into an outer shell that expands very quickly due to the concentrated

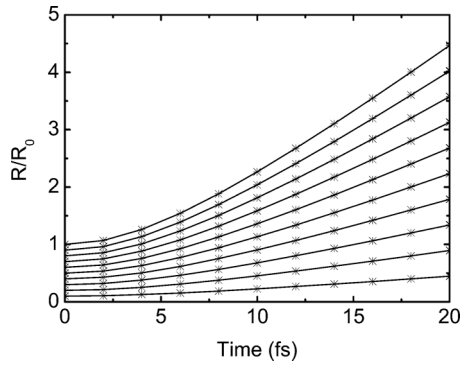

FIG. 6. Comparison of the motions of the atomic shells for the case of a self-similar Coulomb explosion calculated using the analytical model (solid lines) and the numerical computer simulation (stars). The molecule radius is 60 Å and is made of carbon only, no free electrons are present, and the total charge density of 0.22 electrons/Å^3 is initially homogeneous throughout the molecule.

net charge, and an inner core, which is nearly stationary at first and then expands slowly from electron pressure. The expansion of the core is governed by a rarefaction wave that propagates inward at the speed of sound.

Figure 8 shows profiles of the mass density corresponding to the evolution shown in Fig. 7 at different times. A shock wave is present in the outer layers and propagates outward. The shock is due to the change in slope of the radial distribution of the trapped electrons with time. Early in time, the electron distribution is shallower, leading to strong secondary ionization of the outer shells. Simultaneously, the electrons that are present keep the net charge low. At later times, the electron distribution becomes steeper due to the decreasing electron temperature and increased Coulomb forces. This leaves behind a strongly charged layer that experiences a larger acceleration than the outer shells. This leads to the compression of the outer shells inducing a shock wave. Upon further expansion of the molecule the shock wave subsides.

E. Use of molecular tamper to delay motion

The shell/core differentiation seen in Fig. 7 suggests that it is may be possible to encapsulate the molecule in a sacrificial tamper layer, for example water, that will provide extra

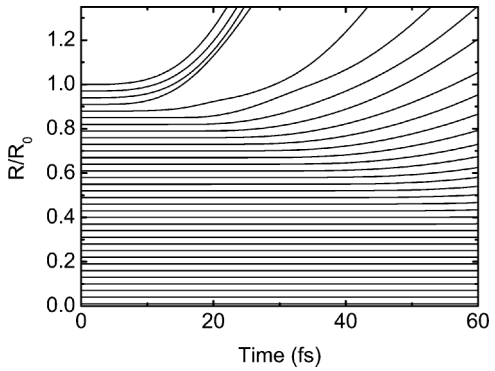

FIG. 7. Motion of the atomic shells for the case of a 60 Å radius molecule illuminated by a photon pulse of flux 1.5×10^{11}ph/fs/(100 nm)^2 for 60 fs. Every 3rd zone boundary is shown.

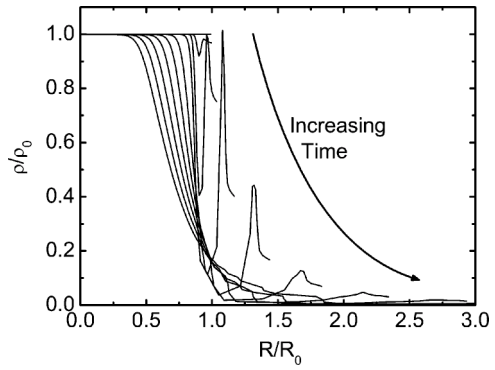

FIG. 8. (a) Profiles of the mass density of a molecule of radius $R_0=60$ Å illuminated by a photon pulse of flux 1.5×10^{11}ph/fs/(100 nm)^2 for 60 fs at different times spaced 6 fs in time apart. The density is normalized to the initial density $\rho_0=1.35$ g/cm^3.

electrons to neutralize the biomolecule and hold back its motion. In this case, the tamper should be approximately 5–10 Å thick. The disadvantages of using a tamper is that the extra electrons will accelerate the ionization of the molecule, and the x-ray scattering from the tamper will generate additional noise in the diffraction image.

F. Parameter survey

We now describe a wide ranging survey covering photon fluxes ranging from 2.5×10^9 to 2.5×10^{11} ph/fs(100 nm)^2 and molecule radii between 20 and 1000 Å. We perform our parameter survey with flat top pulses because the time-dependent results from one simulation can be used to describe the dynamics for any shorter pulse. The use of flat top pulses thereby allows us to consider a wide range of pulse fluences and durations with a reduced parameter study. The results from a flat top pulse are expected to be approximately the same as those for a more realistic pulse shape, such as a Gaussian, provided that the physics of interest occurs on the same time scale as the pulse. First we consider the variation in electron generation with molecular size. Figures 9(a) through 9(e) show the number of trapped and escaped electrons as a function of time for different molecule radii for a flux of 1.5×10^{11} ph/fs(100 nm)^2. Also shown on these graphs are the origins of the trapped electrons. For larger molecules, collisional ionization by secondary trapped electrons dominates over Auger relaxation even more than for smaller molecules. For a 1000 Å molecule, few photoelectrons escape, and the total number of trapped electrons is approximately the sum of photoelectrons and secondary electrons induced by collision. The number of Auger electrons is negligible in this case. For 100 and 150 Å molecules, there is an abrupt increase in the number of electrons at 5 and 2.5 fs, respectively, due to the onset of trapping of photoelectrons. As shown in Fig. 10, the time at which photoelectrons are captured decreases with increasing molecule size since the electrostatic potential, proportional to the total charge over the radius, scales like the square of the radius. Very small molecules cannot build up enough charge to capture photoelectrons at all. This agrees with the temporal evolution of

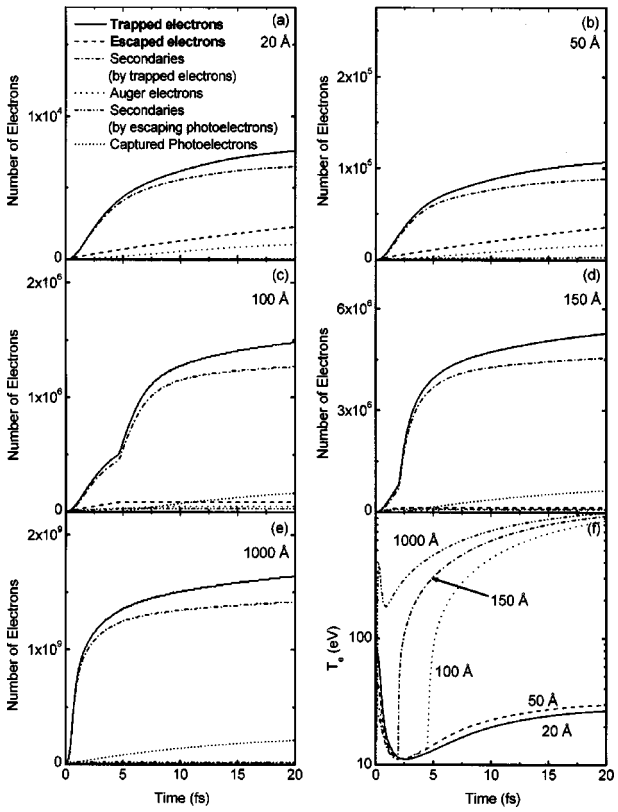

FIG. 9. Number of trapped and escaped electrons as a function of time for different molecule radii (a) 20 Å, (b) 50 Å, (c) 100 Å, (d) 150 Å, and (e) 1000 Å. Also shown on these graphs is the origin of the trapped electrons. (f) Time evolution of the average electron temperature T_e for the same molecule radii. The molecule was illuminated by a photon pulse of flux 1.5×10^{11}ph/fs/(100 nm)^2 for 20 fs.

the average electron energy for different radii as shown in Fig. 9(f). For smaller molecules, the onset of the increase in T_e due to capturing of photoelectrons is later than for larger molecules, and for very small molecules it does not occur at all. Once the high-energy photoelectrons are captured, the atoms are quickly ionized and x-ray diffraction images are expected to be compromised.

To summarize the complete parameter study, we present results for the average ionization and the average atomic mo-

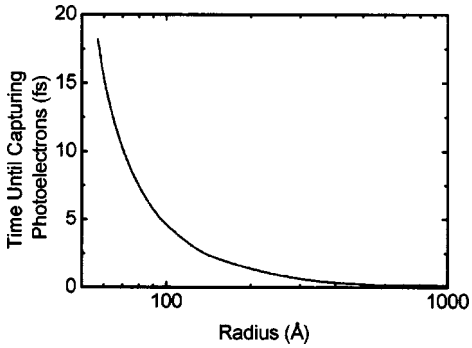

FIG. 10. Time until photoelectrons are captured. We assumed a 60 Å radius molecule illuminated by a photon pulse of flux 1.5×10^{11}ph/fs/(100 nm)^2.

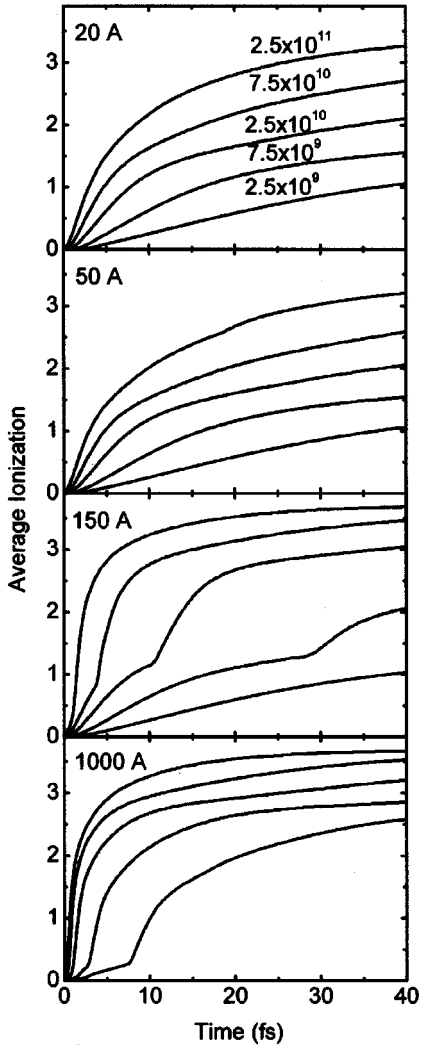

FIG. 11. Temporal evolution of the average atomic ionization, defined as the average number of electrons removed from the atoms, for different molecule radii R, and a range of x-ray fluxes. The x-ray fluxes in units of ph/fs(100 nm)^2 are shown in the top panel.

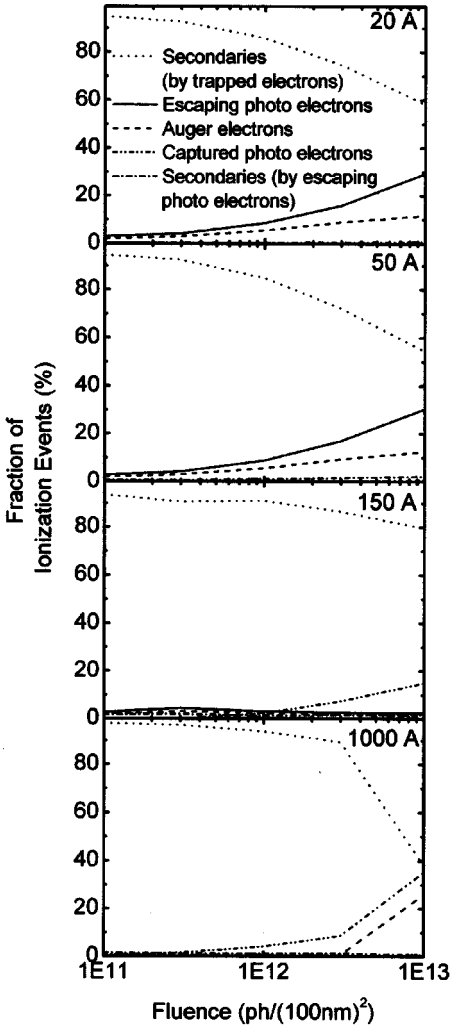

FIG. 12. Origin of ionized electrons for different molecule radii as a function of x-ray fluxes at $t=20$ fs.

tion of the molecules. Figure 11 shows the temporal evolution of the average atomic ionization, defined as the average number of electrons removed from the atoms, for the full set of molecule sizes and x-ray fluxes. The evolution of the average ionization is similar for $R=20$ Å and $R=50$ Å. However, once photoelectrons are trapped, as is the case for $R=150$ Å at fluxes larger than 7.5×10^9 ph/fs/(100 nm)^2, the average atomic ionization abruptly increases. For larger diameter molecules, the trapping of photoelectrons occurs earlier in the pulse as shown in Fig. 10. Therefore, the abrupt increase in ionization occurs sooner, as seen by comparing the $R=150$ Å and $R=1000$ Å cases in Fig. 11.

For all of the cases shown in Fig. 11, average ionization is dominated by collisions. This is apparent from Fig. 12, showing the origin of the ionized electrons for different radii and fluences. Whereas collisional ionization generally dominates, photoionization and Auger ionization become more pronounced for larger fluences. The strong collisional ionization is a very important factor in generating damage to the molecule that may affect the ability to image its structure.

To summarize the atomic motion, we define $f_{\Delta R}$ as the volume fraction of the molecule that is displaced more than a distance ΔR. This quantity gauges the degree to which image resolution would be degraded by the atomic motions. For example, a tolerable volume fraction might be 10% for $\Delta R=2$ Å. The displaced volume fractions are shown in Fig. 13. In the cases where the photoelectrons escape ($R\leqslant 50$ Å and the lower flux cases for $R=150$ Å), a quick Coulomb-induced expansion of the outer charged layers of the molecule leads to a sudden increase in $f_{\Delta R}$. This occurs at times ranging from 7 to 30 fs. Subsequently, $f_{\Delta R}$ increases more slowly due to the hydrodynamic rarefaction wave that propagates inward through the neutralized core. When the photoelectrons are trapped ($R\geqslant 150$ Å for low flux and all cases for $R=1000$ Å) the Coulomb expansion is not as evident and the behavior is dominated by the hydrodynamic rarefaction. This results from the much larger ratio of ionization-to-charge in these cases, making the neutralized core relatively larger. A higher electron temperature also smears out the charged outer layer and makes the Coulomb expansion less apparent. As expected, $f_{\Delta R}$ increases with increasing x-ray fluence, and it tends to be smaller for larger molecules since

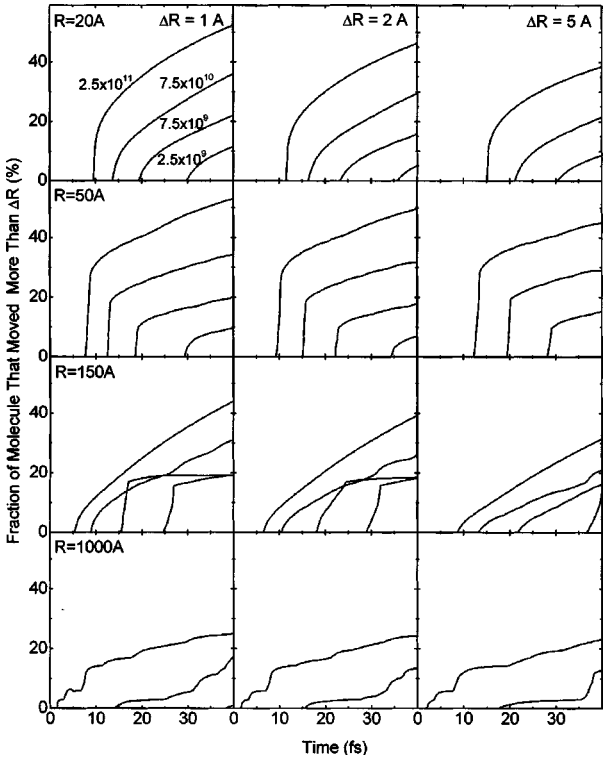

FIG. 13. Temporal evolution of the volume fraction of the molecule that is displaced more than a distance $\Delta R=2$, 3, and 5 Å, for different molecule radii R, and a range of x-ray fluxes. The x-ray fluxes in units of ph/fs$(100\ \mathrm{nm})^2$ are shown in the left top panel.

they trap photoelectrons more easily. Even when the photoelectrons are not trapped, $f_{\Delta R}$ still tends to be smaller for larger molecules because the radial electron distribution is steeper (since the ratio of electrostatic potential energy to electron temperature is bigger), so that a larger fraction of the molecule is Debye shielded.

G. Implications for x-ray imaging

The results for the average ionization and atomic movement are important for determining the maximum pulse length allowed for x-ray imaging of biomolecules. An accurate analysis of this issue requires consideration of the generation of the x-ray diffraction images and the reconstruction of the 3D structures from these images. Here we only make some estimates based on the results presented in Figs. 11 and 13 and on previous estimates of the x-ray fluence required for imaging. The minimum fluence required per single x-ray pulse is set by the requirement of classifying the noisy diffraction patterns according to their angular orientation [10]. To achieve a 3D reconstruction of a 50 Å radius molecule with resolution of 2 Å, the minimum x-ray fluence has been estimated to be approximately 1.0×10^{13} ph/fs/$(100\ \mathrm{nm})^2$. Under these conditions, we find from calculations similar to those presented in Fig. 11(a) but at higher fluxes, that the x-ray pulse length has to be shorter than 0.1, 0.9, and 3.2 fs in order to limit the average atomic ionization to 1, 2, and 3, respectively. We obtained similar results when the effect of three-body recombination was included. Within these short times, there is not sufficient time for the atoms to be displaced by more than 1 Å. Electron trapping and secondary ionization have a strong effect on the damage dynamics of x-ray-irradiated molecules so that the pulse lengths required for x-ray imaging of biomolecules are much shorter than previously suggested [1]. The collisional ionization of the atoms, rather than atomic motion, limits the x-ray pulse length. However, it may be possible to reconstruct the atomic positions from diffraction from highly ionized samples (average ionization $\geqslant3$), since each atom will still retain at least a few tightly bound electrons that will signal the atom's location. In this case, the atomic motions will limit the pulse lengths, and somewhat longer pulses (~5 fs) may be allowed. If a tamping layer is incorporated surrounding each molecule with a thickness of 15% of the radius, longer pulse lengths of ~15 fs may be allowed.

VI. SUMMARY AND DISCUSSION

We have developed a continuum model for the dynamics of x-ray irradiated biological molecules. Our approach has enabled the inclusion of the effect of trapped electrons, and the investigation of very large molecules, exceeding the limitations of molecular dynamics modeling. With this model we have examined the dynamics over a large range of x-ray fluxes and molecular sizes.

We found that trapping of electrons leading to Debye shielding and inhomogeneous ionization has a significant effect on the overall damage kinetics. During the x-ray irradiation, a molecule assumes roughly a two-region structure, consisting of a neutral core and a positively charged outer shell. The shielding greatly reduces the radial atomic motion in the core. The core is damaged primarily through secondary collisional ionization by the trapped electrons. There is less secondary collisional ionization taking place in the outer shells of the molecule since the trapped electrons are primarily confined to the core. The increasing positive charge of the molecule leads to outward motion of the outer shell.

The ionization processes are strongly affected by the trapped electrons. Without trapping, the ionization processes are dominated by photoionization and Auger relaxation. When electrons are trapped by the positive charge of the molecule, these two ionization processes just initiate the damage, and the ionization process is then dominated by collisions. Most of the trapped electrons are generated by collisional ionization by other trapped electrons. A smaller fraction is generated by Auger decay and collisions by escaping photoelectrons.

We also found that ionization is very important and might exceed the significance of damage through radial atomic motion for the photon beam parameters of interest. We estimate pulse lengths required for x-ray imaging of biomolecules on the order of a few femto second, which is much shorter than previously suggested without considering collisional ionization [1]. The incorporation of a tamper layer around the molecule reduces the atomic motion but may lead to ionization damage by providing additional trapped electrons.

Finally, we found that the detailed composition of the molecule has a significant impact on the damage kinetics.

Heavier elements such as sulfur or phosphorous tend to accelerate the damage mechanisms since they easily ionize and quickly provide electrons that are trapped and induce secondary ionization.

ACKNOWLEDGMENTS

We thank D. Miller for showing us a numerical method for solving the hydrodynamic equations, H. Chapman, A. Wootton, J. Hajdu, and B. Ziaja for helpful discussions on several aspects of short pulse x-ray interaction and imaging, and R.W. Lee for drawing our attention to the relevance of three-body recombination. This work was performed under the auspices of the U.S. Department of Energy by the University of California, Lawrence Livermore National Laboratory under Contract No. W-7405-Eng-48.

APPENDIX

In this appendix we present an analytical solution of a simplified expansion dynamics model of an x-ray irradiated particle. In addition to the continuum and spherical assumptions presented in Sec. III, the main assumptions of this model are that the net charge distribution is uniform throughout the molecule, only Coulomb forces act on the matter (no pressure forces), and the x-ray pulse is instantaneous, in essence, much shorter than the dynamical time scale. We call this the pure Coulomb explosion model. The analytical solution can also be extended to include trapped electrons if their temperature is very small compared to the escape temperature. The analytical solution provides a general understanding of the explosion dynamics and is also useful to check numerical methods used for the more general model discussed in the body of the paper.

We start by defining Q as the net positive charge produced on the molecule by an extremely short pulse of x rays. The net charge is due to photoionization and may also include Auger ionization when the dynamical time scales are longer than the Auger decay time. The charge Q can be calculated from the x-ray absorption cross sections of the atoms and the x-ray fluence, as discussed in Sec. III in connection with the ionization rate equations. We assume that the molecule is initially a homogeneous sphere, conceptually partitioned into infinitesimal shells, each identified by its initial radius r_o. The trajectory of each shell can be found from the energy form of the classical equation of motion:

$$\frac{dr}{dt} = \sqrt{\frac{2}{m}(E-U)}. \tag{A1}$$

Here m is the mass per unit charge, and E and U are, respectively, the total energy and potential energy, each per unit charge. Consistent with the spherical, uniform charge density approximation, $U=eQ(r_o/R)^3/4\pi\varepsilon_0 r$. Since the matter starts at rest, $E=U(r_o)$.

Since the right-hand side of Eq. (A1) is a function only of r, it can be integrated to obtain an implicit solution for the trajectory of each shell:

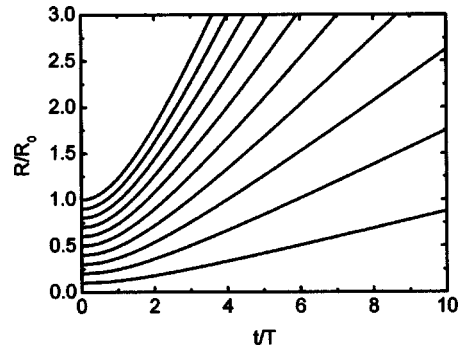

FIG. 14. Trajectories of ten radial shells in the analytic model. The shells originate at radii between $0.1R$ and R. Time is measured in units of the characteristic time, $T=(4\pi\varepsilon_o)^{1/2}(2\pi\rho/3)^{1/2}R^3/Q$.

$$t = (4\pi\varepsilon_o)^{1/2}\left(\frac{2\pi}{3}\rho\right)^{1/2}\frac{R^3}{Q}\frac{1}{r_o}I, \quad \text{where}$$

$$I \equiv \int_{r_o}^{r}\frac{x^{1/2}dx}{(x-r_o)^{1/2}} = r^{1/2}\sqrt{r-r_o} + r_o \ln\left(r^{1/2}+\sqrt{r-r_o}\right) - r_o\ln(r_o^{1/2}) \tag{A2}$$

and ρ is the initial mass density of the molecule.

Figure 14 shows solutions of Eq. (A2). We see that the motion is self-similar in that all shells begin to move at the same time and they follow trajectories of the same shape.

We are mainly interested in small displacements, $\Delta r \ll R$, since we strive to determine the molecular structure at much higher resolution than the initial radius. We concentrate on the surface since it moves the fastest and thereby provides the most stringent constraint on the pulse length. We find in this case

$$\mathrm{t} = \left(\frac{2\pi}{3}\rho\, R\right)^{-1/2}\frac{M_a}{f_i}\frac{(4\pi\varepsilon_0)^{1/2}}{e}\sqrt{\Delta r} = 5.3\ \mathrm{fs}\left[\left[\rho\left(\frac{R}{10\ \text{Å}}\right)\right]^{-1/2}\left(\frac{M_a}{7}\right)(f_i)^{-1}(\Delta r)^{1/2}\right], \tag{A3}$$

where M_a is the average mass per atom (in atomic units), e is the electron charge, ρ is the density in $\mathrm{g/cm^3}$, and f_i is the fraction of atoms that are ionized. The value of M_a is approximately equal to 7 for typical biological molecules.

As discussed in Sec. II, a significant number of electrons may be trapped in the average electrostatic field of the molecule. With trapped electrons, the molecule will assume a two-zone structure with a neutral interior core and a positively charged shell around the core. The width of the transition between the core and the charged shell depends on the ratio of the electron temperature to the escape energy. By assuming that the electron temperature is very small compared to the Coulomb escape potential, the length of this transition region is much smaller than the radius of the molecule. In this case we can extend the analytical solution given in by Eq. (A2) to include the effect of trapped electrons. Defining β as the ratio of the number of trapped electrons to the number of escaping electrons, we find that the

charged shell has a volume equal to $1/(1+\beta)$ times the volume of the molecule, and a charge density equal to $(1+\beta)$ times the mean positive charge density. Typical values of β are $1-10$, as deduced from the results presented in Sec. V. The expansion time for the material in the outer shell is $(1+\beta)^{-1/2}$ times that given by Eqs. (A2) and (A3). The trapped electrons cause the outer shell to expand faster, while the inner core is neutralized and does not expand at all when considering only the electrostatic forces. Considering a finite electron temperature the inner core will expand on a longer time scale via a hydrodynamic rarefaction, as discussed in Sec. V and illustrated in Fig. 7.

[1] R. Neutze, W. Wouts, D. van der Spoel, E. Weckert, and J. Hajdu, Nature (London) **406**, 752 (2000).
[2] R. Henderson, Q. Rev. Biophys. **28**, 171 (1995).
[3] J. Arthur *et al.*, Linac Coherent Light Source (LCLS) Design Study Report No. SLAC-R-521, 1998 (unpublished), also available online at: http://www-ssrl.slac.stanford.edu/lcls/design_report/e-toc.html
[4] J. C. Solem and G. F. Chapline, Opt. Eng. **23**, 193 (1984).
[5] J. C. Solem and G. C. Baldwin, Science **218**, 229 (1982).
[6] Ya. S. Derbenev, A. M. Kondratenko, and E. L. Saldin, Nucl. Instrum. Methods Phys. Res. **A193**, 415 (1982).
[7] J. B. Murphy and C. Pellegrini, J. Opt. Soc. Am. B **2**, 259 (1985).
[8] R. F. Service, Science **298**, 1356 (2002).
[9] F. Richard, J. R. Schneider, D. Trines, and A. Wagner, TESLA Technical Design Report No. 2001-11, 2001 (unpublished), available at the web site http://tesla.desy.de/new_pages/TDR_CD /start.html.
[10] G. Huldt, A. Szoke, and J. Hajdu, J. Struct. Biol. **144**, 219 (2003).
[11] R. Gerchberg and W. Saxton, Optik (Jena) **35**, 237 (1972).
[12] S. P. Hau-Riege, H. Szoke, H. Chapman, A. Szoke, S. Marchesini, A. Noy, H. He, M. Howells, U. Weierstall, and J. C.H. Spence, Acta Cryst. A (to be published).
[13] Z. Jurek, G. Faigel, and M. Tegze, Phys. Rev. B (to be published); Z. Jurek, G. Oszlanyi, and G. Faigel, Europhys. Lett. **65**, 491 (2004).
[14] E. J. McGuire, Phys. Rev. **185**, 1 (1969).
[15] D. A. Verner, D. G. Yakovlev, I. M. Band, and M. B. Trzhaskovskaya, At. Data Nucl. Data Tables **55**, 233 (1993).
[16] B. Ziaja, A. Szoke, D. van der Spoel, and J. Hajdu, Phys. Rev. B **66**, 24 116 (2002).
[17] B. L. Henke, E. M. Gullikson, and J. C. Davis, At. Data Nucl. Data Tables **54**, 181 (1993).
[18] M. A. Lennon, K. L. Bell, H. B. Gilbody, J. G. Hughes, A. E. Kingston, M. J. Murray, and F. J. Smith, J. Phys. Chem. Ref. Data **17**, 1285 (1988).
[19] K. L. Bell, H. B. Gilbody, J. G. Hughes, A. E. Kingston, and F. J. Smith, J. Phys. Chem. Ref. Data **12**, 891 (1983).
[20] Y.-K. Kim and M. E. Rudd, Phys. Rev. A **50**, 3954 (1983).
[21] S. Chelkowski and A. D. Bandruk, J. Phys. B **28**, L723 (1995).
[22] B. Ziaja, A. Szoke, R. A. London, and J. Hajdu (unpublished).
[23] R. D. Richtmyer and K. W. Morton, *Difference Methods for Initial-Value Problems*, 2nd ed. (Krieger Publishing, Melbourne, 1994).
[24] J. von Neumann and R. D. Richtmyer, J. Appl. Phys. **21**, 232 (1950).
[25] E. J. Caramana, M. J. Shahkov, and P. P. Whalen, J. Comput. Phys. **144**, 70 (1998).
[26] R. Courant, K. O. Friedrichs, and H. Lewy, Math. Ann. **100**, 32 (1928).
[27] W. H. Press, B. P. Flannery, S. A. Teukolsky, and W. T. Vetterling, *Numerical Recipes in C*, 2nd Ed. (Cambridge University Press, Cambridge, 1993).
[28] H. M. Berman, J. Westbrook, Z. Feng, G. Gilliland, T. N. Bhat, H. Weissig, I. N. Shindyalov, and P. E. Bourne, Nucleic Acids Res. **28**, 235 (2000).
[29] H. R. Griem, *Principles of Plasma Spectroscopy* (Cambridge University Press, Cambridge 1997), p. 167–172.